Taylor & Francis
Taylor & Francis Group

Comparison between *in situ* and MODIS-derived spectral reflectances of snow and sea ice in the Amundsen Sea, Antarctica

X. ZHOU* and S. LI

Geophysical Institute, University of Alaska Fairbanks, PO Box 757320, Fairbanks, AK 99775-7320, USA

Abstract. The spectral albedo and directional reflectance of snow and sea ice were measured on sea ice of various types, including nilas, grey ice, pancake ice, multi-year pack ice, and land-fast ice in the Ross, Amundsen and Bellingshausen seas during a summer cruise in February through March 2000. Measurements were made using a spectroradiometer that has 512 channels in the visible and near-infrared (VNIR) region in which 16 of the 36 bands of the Moderate Resolution Imaging Spectroradiometer (MODIS) are covered. Directional reflectance is also retrieved from the MODIS radiometrically calibrated data (Level 1B) concurrently acquired from the first National Aeronautics and Space Administration (NASA) Earth Observing System (EOS) satellite, Terra. The locations of the ground ice stations are identified accurately on the MODIS images, and the spectral albedo and directional reflectance values at the 16 VNIR MODIS bands are extracted for those pixel locations. MODIS-derived reflectance is then corrected for the intervening atmosphere whose parameters are retrieved from the MODIS atmospheric profiles product (MOD07_L2) for the same granule. The corresponding spectral albedo and directional reflectance with the same viewing geometry as MODIS are derived from our ground-based spectroradiometer measurements. Because the footprint of the ground spectro-radiometer is much smaller than the pixel sizes of MODIS images, the averaged spectral reflectance and albedo in the vicinity of each ice station are simulated for the corresponding MODIS pixel from the ground spectral measurements by weighting over different surface types (various ice types and open water). An accurate determination of ice concentration is important in deriving ground reflectance of a simulated pixel from *in situ* measurements. The best agreement between the *in situ* and MODIS measurements was found when the ground had 10/10 ice concentration (discrepancy range 0.2–11.6%, average 4.8%) or was one-ice-type dominant (discrepancy range 0.8–16.9%, average 6.2%). The more homogeneous the ground surface and the less variable the ground topography, the more comparable between the *in situ* and satellite-derived reflectance is expected.

---

*Corresponding author. Present address: Department of Earth and Environmental Science, New Mexico Tech, Leroy Place 801, Socorro, NM 87801, USA; e-mail: xiaobing@ees.nmt.edu.

1. Introduction

Albedo of snow and ice surface in the polar regions is a sensitive parameter in the study of climate. Because the energy stored at the Earth's surface and in the atmosphere comes primarily from the solar radiation, albedo is an important boundary condition for energy budget between the atmosphere and the Earth (Sellers 1969). As satellites can provide temporally repetitive coverage and spatially continuous data in the polar regions that are not easily accessible for ground-based measurements, monitoring the surface change for the climate change study depends increasingly on satellite remote sensing (Stroeve *et al.* 1997, 2001, Lucht *et al.* 2000).

A direct comparison between the satellite-derived and *in situ* measurement is generally difficult when the ground surface is very heterogeneous. For instance, the difference can be as large as 30% (Hall *et al.* 1992) for glacier ice during summer melt and 11% for an ice sheet with 20% melt pond coverage (Stroeve *et al.* 1997). Comparison of satellite sensor data with *in situ* measurement over pack ice in polar seas is even more difficult because of two reasons. Firstly, the pack ice in polar seas is a dynamic Earth surface which is in constant motion and deformation, and thus no 'permanent' ground data exist. Secondly, sea ice is very heterogeneous and a satellite pixel generally covers more than one ice type and different types of ice have distinctive reflectivity. To overcome these difficulties, our strategy is as follows:

- *In situ* measurements are completed as exactly concurrent as possible with the Moderate Resolution Imaging Spectroradiometer (MODIS) overpasses to avoid ground data shift due to ice motion. At each ice station on which the reflectance measurement is concurrent with the Terra satellite overpass, the ice types and ice concentration are coincidentally observed and recorded with *in situ* reflectance observations.
- The small angle approximation (Nishihama *et al.* 1997) and the direct matching algorithm are used (Patt *et al.* 1997) to improve the navigation accuracy. To locate the ground site in the imagery accurately and quickly, the scan and frame numbers (line and column position) of ground site are first estimated using the small angle approximation. Then, the accurate location is identified using the direct matching algorithm.
- Ice concentration and reflectance of various ice types are used to correct the ground measurement over a simulated pixel the same size as MODIS. Measurements of reflectance are carried out on as many ice types as possible that cover the main ice types met along the ship-track during the cruise.

The use of the MODIS data to retrieve the ground surface geophysical and biophysical parameters requires atmospheric correction so that the top of the atmosphere (TOA) radiance can be converted to the actual ground surface reflectance. The ground surface reflectance with atmospheric effects corrected is an estimate of the surface reflectance for the given atmospheric condition based on the TOA radiance received by the satellite sensor. Adequate atmospheric correction requires an accurate description of the profile of the variable constituents of the atmosphere that influence the TOA radiance received by the satellite sensor, and a correct modelling of the absorption and scattering of solar radiation by the atmosphere. Two methods are generally used for the atmospheric correction. One is the correction scheme based on satellite-measured radiances at the TOA (Dave and Gazdag 1970, Reijmer *et al.* 2001). The basis of this kind of scheme is that the

attenuation of the solar radiance due to the intervening atmosphere is exponentially attenuated (Liljequist 1956, Schlatter 1972, Reijmer *et al*. 2001). The attenuation coefficient or the optical depth is obtained beforehand by use of comprehensive radiative transfer models (Dozier and Marks 1987, Koepke 1989) so that the atmospheric correction is possible. The accuracy of the correction depends on the accuracy of the optical depth. This method is widely used because of its simplicity, especially for clear sky conditions (Hall *et al*. 1990, De Abreu *et al* 1994, Knap and Oerlemans 1996, Zhou *et al*. 2001). The alternative method for atmospheric corrections is the use of comprehensive radiative transfer models such as 6S (Tanré *et al*. 1992, Vermote *et al*. 1997a, b), considering the absorption and scattering by the main components of the atmosphere.

The MODIS instrument on Terra satellite was designed to provide improved monitoring of the Earth for land, ocean and atmospheric research and to meet the needs of global change research. MODIS data products are categorized into five levels in order of increasing level of processing. Level 1B (L1B) products are generated from the raw instrument data (Level 0) by appending geolocation and radiometric calibration data. Multiple onboard calibration systems are used in the MODIS instrument to ensure a calibration accuracy of 2% relative to the solar radiance (Guenther *et al*. 1998). The MODIS surface reflectance product, MOD 09, is a seven-band product computed from MODIS L1B land bands 1, 2, 3, 4, 5, 6 and 7. Although this product is atmospherically corrected, only three bands are covered by the spectroradiometer (330–1060 nm), which covers 16 bands of the 20 MODIS visible and near-infrared (VNIR) bands. Thus, we used the L1B product, and the atmospheric corrections for the 16 VNIR MODIS bands covered by the ground-based spectroradiometer were accomplished using a modified 6S radiative transfer code as described in the manuscript.

In this paper, the comparison is made between the 1 km MODIS-derived surface reflectance and that measured *in situ* concurrently on the snow and sea ice surface. With validation of MODIS sea ice products as the primary purpose, we participated in a cruise to the Ross, Amundsen and Bellingshausen seas, Antarctica onboard US R/V Nathaniel B. Palmer, February and March 2000 (figure 1). Measurements at 22 ice stations were made. Among the 22 daily measurements, three measurements from three Julian days shown in figure 1 were recorded under 'very clear' sky conditions. All three sites are in the Amundsen Sea and are chosen for detailed comparison and analyses in this study.

2. Surface reflectance from ground measurements

Ground measurements are used to assess the accuracy of MODIS-derived reflectance in discrete reflective spectral bands. The time to make the daily *in situ* measurements was in line with an overpass time schedule of satellite Terra obtained beforehand, so that simultaneous *in situ* data and MODIS data were acquired. Study sites are shown in figure 1, with the Julian days indicated. The cruise track is shown in the inset map, with the ice station number explicitly noted. As many ice types as possible were taken as platforms for our reflectance measurements. Based on the field observations, ice types upon which the measurements were made are categorized into land-fast ice, multi-year year (MY) ice, first year (FY) young white ice, new ice of 5–10 cm thick including cemented pancake ice and young grey ice, and new ice of 2–4 cm thick including pancake ice and nilas.
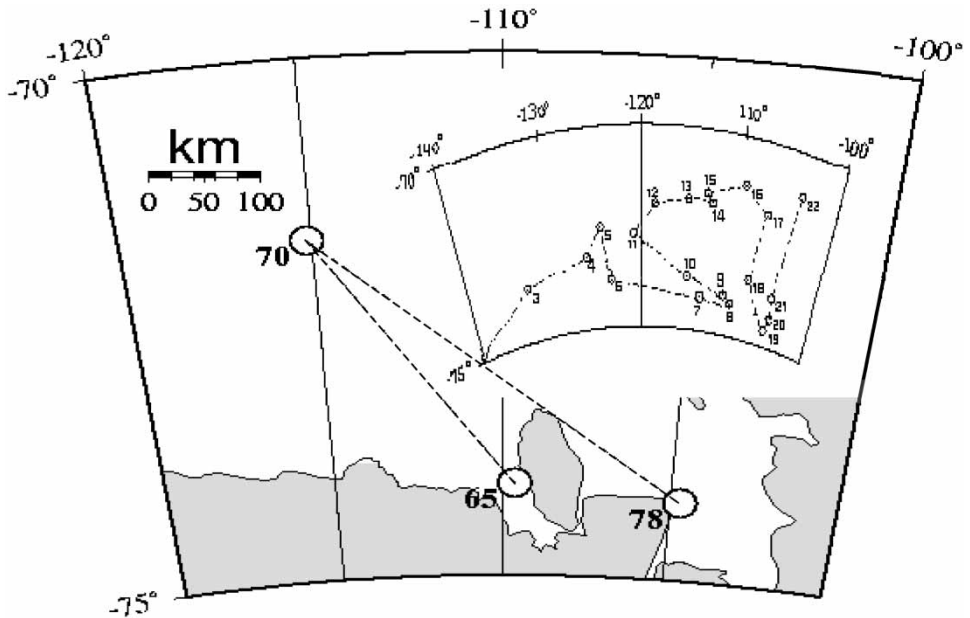
Figure 1. Field study sites on the pack ice in the Amundsen Sea. Numbers are the corresponding Julian days in year 2000. Inset map shows the NBP-01 cruise tract and ice station (open circle) number in the Amundsen and Bellingshausen seas. The first two ice stations in the Ross Sea are not shown.

2.1. *Direct ground measurement*

Spectral albedo and directional reflectance of snow and sea ice were measured at each ice station. Spectral albedo was measured using a high-spectral-resolution fibre optic spectroradiometer manufactured by Analytical Spectral Devices, Inc. (ASD). The spectroradiometer measures spectral reflectance and spectral radiance at 512 spectral bands from 333.65–1064.9 nm, with a spectral resolution of 3 nm. Sixteen of the 36 bands of the Terra MODIS are covered in the 512 channels in the VNIR region. The spectral albedo measurement was performed with the spectroradiometer and a remote cosine receptor (RCR) of a hemispherical field of view (FOV). The instrument set-up was the same as described previously (Zhou *et al.* 2001). The spectral albedo was acquired by measuring the downwelling spectral irradiance, followed immediately by measuring the upwelling spectral irradiance using the RCR. To reduce the system errors and errors caused by the fluctuations of the radiation field, several samples, each being the average of 10 scans, for both upwelling and downwelling spectral irradiances were collected.

Among the 22 ice stations, 14 measurements of spectral albedo were made, of which seven were on MY ice floes, three on new grey ice (5–10 cm thick), one on FY young white ice, two on new ice (2–4 cm thick) and one on land-fast ice. The cruise was a multi-purpose mission. Time allocated to each science group onboard was limited at each ice station. Exhaustive reflectance measurements of all ice types at one ice station within one imagery pixel had not been possible. The ice in the Amundsen Sea was predominantly MY ice (survived at least one summer) in the later summer/early autumn of the year. Young white ice was seldom met during the

cruise, and new ice was beginning to form at this stage. Thus the number of measurements on young white ice and new ice was very limited. As the Ross and Amundsen seas are the least studied areas in the southern ocean, we do not have any reference data available in literature with which we can compare our measurements. However, from our seven measurements (seven MY ice stations) of the MY ice, the maximum deviation of spectral albedo is 3.8%, occurring at 1.06 μm. For FY ice (including young white ice and young grey ice), the variation of spectral albedo at a specific region is expected to be smaller than the MY ice due to the FY ice being less heterogeneous (Gogineni *et al.* 1992). Therefore, the contribution to the concentration correction of *in situ* reflectance from the variation of spectral albedo of young white ice and new ice is likely to be small. Thus, the average of the measured data for the same ice type through the whole cruise is used for the ice-type to make the ice concentration correction to the ground reflectance at a simulated pixel of 1 km MODIS spatial resolution. Reflectance obtained this way is called ice concentration weighted or ice concentration corrected ground reflectance at satellite spatial resolution.

For this study, only four types of ice are typical for the ice stations of days 65, 70 and 78, and the spectral albedos of these ice types are shown in figure 2. Based on these measurements, the spectral albedos of bands corresponding to the MODIS sensor are extracted and put into a look-up table (LUT) for the calculation of the ground bidirectional reflectance at the spatial resolution of 1 km. This LUT is given in table 1 and is used in §2.2 to calculate ice concentration weighted ground reflectance. Within the ice types shown in figure 2, MY ice is generally associated with deepest snow and a fine snow grain-size, thus it has the highest spectral albedo.
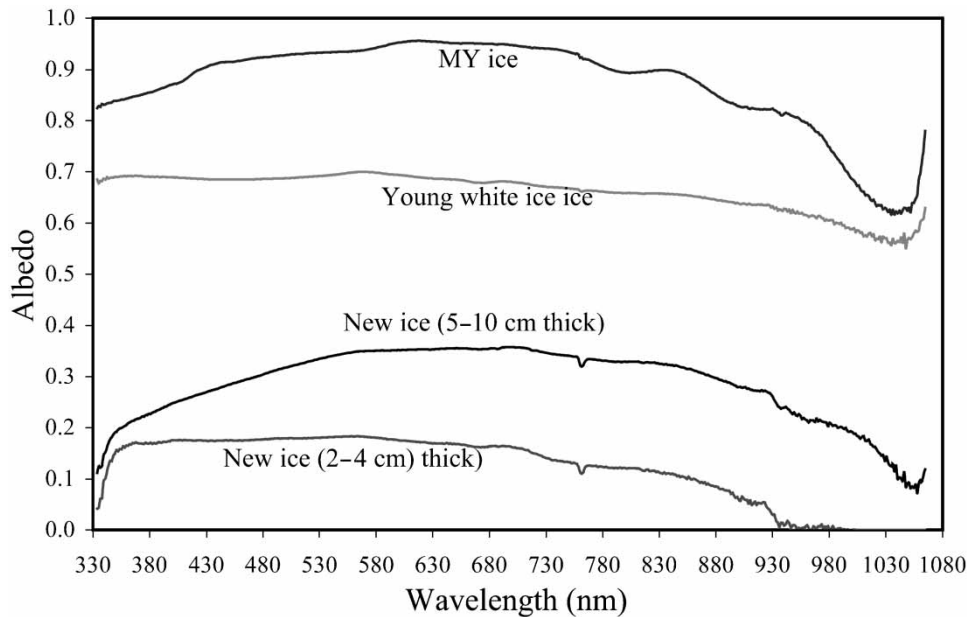
Figure 2. Spectral albedo for different ice types measured in the Ross, Amundsen and Bellingshausen seas from the 2000 cruise. Each curve corresponds to the average of all measurements on the same ice type.

Table 1. Look-up table for the concentration-correction of reflectance at MODIS bands covered by the ground spectroradiometer.

MODIS band	MY ice	FY white ice	New ice (5–10 cm)	New ice (2–4 cm)
1	0.951	0.685	0.356	0.169
2	0.883	0.653	0.314	0.100
3	0.920	0.685	0.296	0.176
4	0.935	0.697	0.346	0.183
8	0.881	0.687	0.256	0.175
9	0.913	0.685	0.278	0.175
10	0.925	0.686	0.310	0.178
11	0.933	0.692	0.335	0.181
12	0.934	0.696	0.344	0.183
13	0.949	0.680	0.353	0.164
14	0.950	0.679	0.354	0.162
15	0.935	0.668	0.341	0.133
16	0.867	0.649	0.306	0.092
17	0.826	0.638	0.279	0.060
18	0.815	0.626	0.240	0.007
19	0.813	0.626	0.239	0.010

New ice (2–4 cm thick), including pancake ice and nilas, frequently has liquid water on the surface and seldom has snow atop. As a result, it has the lowest spectral albedo.

Directional reflectance measurements were carried out using the spectro-radiometer and a fore-optic sensor of 3° FOV. The measurement of bidirectional reflectance proceeded in a similar fashion to that previously described by Zhou and Li (2000). At each fixed viewing zenith angle (beginning at nadir), measurements were carried out in the azimuth domain at 10° intervals from the forward scattering direction in the principal plane (relative azimuth angle $\varphi = 180°$) to the backward scattering direction ($\varphi = 0°$). After each scan in the azimuth, the viewing zenith angle was increased by 10° for a new scan in the azimuth up to 80°. The same viewing geometry as the MODIS sensor is later interpolated from the set of measurements at multiple view angles after the satellite viewing geometry has been retrieved from the MODIS radiometric calibration product (L1B) so that the *in situ* and satellite-retrieved reflectance can be directly compared without the necessity of a viewing geometry correction (Jin and Simpson 2000).

The ice concentration was estimated by observation from the bridge of the research vessel. According to a technique of ship-based observation of sea ice characteristics (Worby and Allison 1999), at most three dominant ice types and open water (OW) were identified for one observation. Ice type, ice concentration and OW concentration were recorded. For the station where more than three ice types were present, the most optically (visually) similar types were grouped and amalgamated into one of the three categories. Data obtained by ship-based observation were blended with the field images taken coincidentally using a digital camera and the final types and concentration data for each measurement site were obtained. The data for the three measurement sites are given in table 2. Measurements of spectral albedo and bidirectional reflectance were taken on the primary (most concentrated) ice type floe. For the site of day 65, the ice concentration was 10/10. Reflectance was measured on the MY ice that was the

Table 2. Ice types and concentrations at each of the three daily stations.

	Day station		
	65	70	78
Primary ice type (concentration)	MY (6/10)	MY (4/10)	Young grey ice (3.5/10)
Second ice type (concentration)	Young white ice (3/10)	New ice (5–10 cm) (3/10)	–
Third ice type (concentration)	New ice (5–10 cm) (1/10)	–	–
OW concentration	0/10	3/10	6.5/10

MY = multiyear ice; OW = open water.

Ice concentration of a specific type of ice is the areal coverage of the ice type over the whole area visible, expressed in tenths.

dominant type (6/10). Young white ice (3/10) was the second ice type. New ice (nilas) (5–10 cm thick) accounted for only 1/10. As both the young white ice and MY ice are very reflective, this site was characterized as a very reflective surface. On the site of day 70, only two ice types existed. MY ice was the dominant (4/10) over the new ice (nilas and pancake ice) (5–10 cm thick). Measurements were made on the MY ice. The site of day 78 was the simplest of the three. Only one ice type existed. Ice concentration of the young grey ice was just 3.5/10.

2.2. *Ice concentration corrected* in situ *reflectance*

A simulated pixel often contains more than one type of sea ice. A reflectance measurement was usually taken on one representative ice floe. Based on the statistical results of spectral albedo measurements for various sea ice types shown above, the concentration correction scheme of the *in situ* reflectance is as follows

$$R_{correct} = f_1 R_{measured} + f_2 R_2 + f_3 R_3 + (1 - f_1 - f_2 - f_3) R_{water} \tag{1}$$

where $R_{correct}$ is the *in situ* reflectance corrected for ice concentration; $R_{measured}$ is the directly measured reflectance at a specific viewing angle on the primary ice type; f_1, f_2, f_3 are the concentrations of the primary, secondary and tertiary ice types respectively; and R_2, R_3 and R_{water} are the reflectances of the secondary ice type, tertiary ice type and OW, respectively. The fourth term on the right-hand side is from the contribution of OW. R_2, R_3 and R_{water} are not, however, available at each site. To circumvent the unavailability, the general spectral albedo database presented in table 1 is used for replacement. Spectral albedo of water is taken from Allison *et al.* (1993) for its directional reflectance. This simplification is equivalent to neglecting the anisotropy of reflectance of the secondary and tertiary ice types and open water. Although this will cause deviations for the calculated reflectance from the actual reflectance (Knap and Reijmer 1998, Warren *et al.* 1998, Greuell and de Ruyter de Wildt 1999), when insufficient knowledge of anisotropy of the surface is available, isotropic reflectance is assumed. For this reason, it is still widely used in the conversion of narrowband satellite reflectance to broadband albedo (Duguay and LeDrew 1992, Gratton *et al.* 1993, Knap *et al.* 1999). Besides, errors resulting from the isotropic assumption in concentration corrected reflectance in equation (1) depends largely on the representativity of the primary ice type within
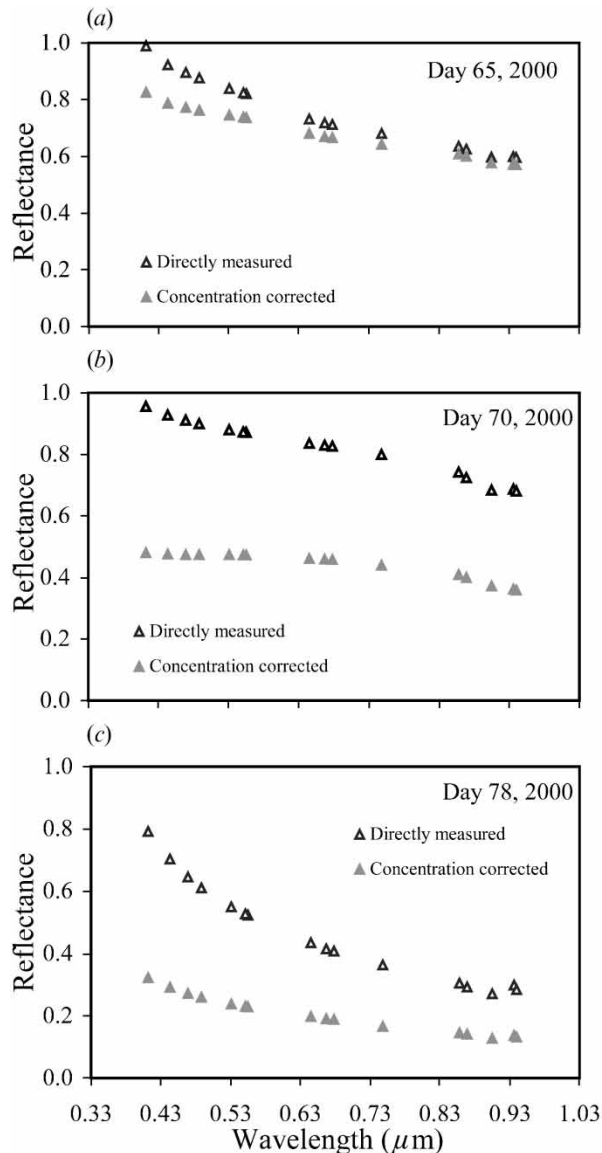
Figure 3. Directly measured and concentration weighted bidirectional reflectances for the three ground sites shown in figure 1: (*a*) day 65, (*b*) day 70 and (*c*) day 78, 2000.

the pixel on which *in situ* reflectance was made. The higher the concentration of the primary ice type, the smaller the errors resulting from this simplification.

Differences between the directional reflectances directly measured and concentration weighted for the three sites are shown in figure 3. At the station of day 65, ice concentration was 10/10, with the primary ice type being the dominant one (table 2). The correction is mainly in the blue light bands. The average correction of the 16 bands is 8.5%, with the largest correction (16.5%) occurring at band 8 (412 nm) and the smallest correction (3.3%) at band 17

(905 nm). At the measurement site on day 70, ice concentration was 7/10, with primary ice type (MY ice) 4/10 and new ice (5–10 cm thick) 3/10. The average correction for the 16 bands is 46.3%, with the largest correction (49.8%) at band 8 (412 nm) and the least correction (44.6%) at band 14 (678 nm). For this site, although the measurement was made on the most reflective type of ice, yet the concentration of the primary ice type is small (4/10), and the correction is remarkable. The shapes of the spectral reflectance before and after the concentration correction are quite similar if the primary ice type is overwhelmingly dominant in reflection. For the site of day 78, ice concentration was only 3.5/10; correction is large for all bands as it is on day 70's site. As only one ice type is available, correction for this case is simple. The average correction from the directly measured reflectance is 55.3%, with the largest correction (59.3%) occurring at band 8 (412 nm) and the smallest (51.7%) at band 16 (869 nm). The shapes of the spectral reflectance before and after the concentration correction are quite similar, just as in day 70.

3. Matching algorithm of a ground station position within a MODIS imagery granule

The MODIS datasets used for this comparative study are the MODIS L1B 1 km Earth-view (EV) product (Guenther *et al.* 1998) and the MODIS Atmospheric Profiles product (MOD07_L2) (Menzel and Gumley 1998). Both products are stored in granules that are derived from approximately five minutes of continuous instrument data in the Hierarchical Data Format for Earth Observing System (HDF-EOS). Reflectance of the ground surface is retrieved from the L1B products and the atmospheric parameters for atmospheric correction are retrieved from the MOD07_L2 products for the same granule.

For satellite measurements to be comparable with the ground measurements, one important step is to locate correctly the ground site in the imagery. For MODIS L1B 1 km products, the scientific datasets (SDSs) are generally 2030 (scan lines) × 1354 (frames). These data are not geometrically rectified and registered to a conventional map projection, thus the ground size of each pixel changes with its pixel location. Data collected at nadir have a nominal spatial resolution of 1 km and this becomes coarser with distance off nadir. The instantaneous ground spatial resolution expands by a factor of four towards the end of each scan ($\pm 55°$) due to the Earth curvature. In this paper, when a pixel is referred to the ground surface, it is referred to the ground FOV of a single detector sample from one of the 1 km nadir spatial resolution MODIS bands. The geographical datasets in the L1B products are used for the geolocation of the ground site in the imagery. For each ground pixel in MODIS L1B products, the ground height and zenith angles are measured with respect to the local ellipsoid normal, and the azimuth angles are relative to local geodetic north.

MOD07_L2 product consists of total-ozone burden, atmospheric stability, temperature and moisture profiles, and atmospheric water vapour. All of these parameters are produced at a 5 km × 5 km pixel spatial resolution when at least nine of the 25 1 km sub-pixels are cloud free. The corresponding geographical datasets for a L1B granule is 406 (lines) × 271 (frames), each point representing a 5 × 5 pixel subset in the L1B SDSs. The mapping relationship between MODIS L1B product

and MOD07_L2 product for the same granule is given by

$$n_s = 5(n'_s - 1) + 3$$
$$n_f = 5(n'_f - 1) + 3$$

$$(2)$$

where n_s and n_f are the scan line number and frame number in the SDSs of L1B product and n'_s, n'_f are the line number and frame number in the corresponding geographical datasets for the same granule. Equation (2) is used to retrieve atmospheric parameters from the pixel in the MOD07_L2 product that contains the ground site.

The retrieval processes of pixel location for the ground sites include the following main steps:

(1) estimating the approximate scan line number and frame number of the pixel that contains the ground measurement site. This is accomplished by the inverse mapping algorithm that for a given ground point in geodetic coordinates (latitude and longitude) the matching pixel within a MODIS imagery granule (Nishihama *et al.* 1997) will be found;

(2) extracting a small candidate pixel patch around the estimated pixel obtained in the first step;

(3) applying a direct match method to locate accurately the pixel that contains the measurement site (Patt *et al.* 1997). If the optimal pixel lies at the edge of the patch, shift the patch so that it centres at the newly optimal pixel. This process continues until the optimal pixel lies inside the patch.

Figure 4 shows the flow chart of the above processing methodology to locate ground station position in the MODIS imagery granule.

The pixels found to match the ground stations and the distances between the station position and the centre of the pixel are shown in table 3. The design of the Earth location algorithm which generates the Earth location data was dictated by the accuracy requirement that the Earth location data are accurate to 0.1 pixel (Nishihama *et al.* 1997); the geolocation error is expected to be 100 m for the nadir pixels. The spatial resolution of the pixel at nadir is 1 km, a pixel off nadir has coarser spatial resolution. As the distance between the ground site and the centre of the imagery pixel is less than 0.707 km for the imagery granules of day 65 and day 70, it is evident that the ground stations lie well within the pixels. For day 78's granule, the distance is over 1 km. However, considering that the pixel is very much off nadir, and the pixel size is larger than 2 km, the ground site is still within the pixel.

4. Ground reflectance retrieved from MODIS data

Once the pixel is found, WebWinds (an interactive science data visualization system) (Elson *et al.* 2000) is used to display the scaled integer (SI) for all the bands of the pixel from the SDSs along with the reflectance scale and offset from the SDSs attributes and solar zenith angle from the global attributes of the granule. Then, reflectance can be calculated from equation (3). Reflectance obtained this way is the apparent reflectance at the TOA, without the atmospheric correction. However, atmospheric disturbance on the reflectance measured at satellite platforms is far from being negligible; as much as 20% is possible (Stroeve *et al.* 1997), especially in the shortwave bands. To compare with the ground measurements, atmospheric
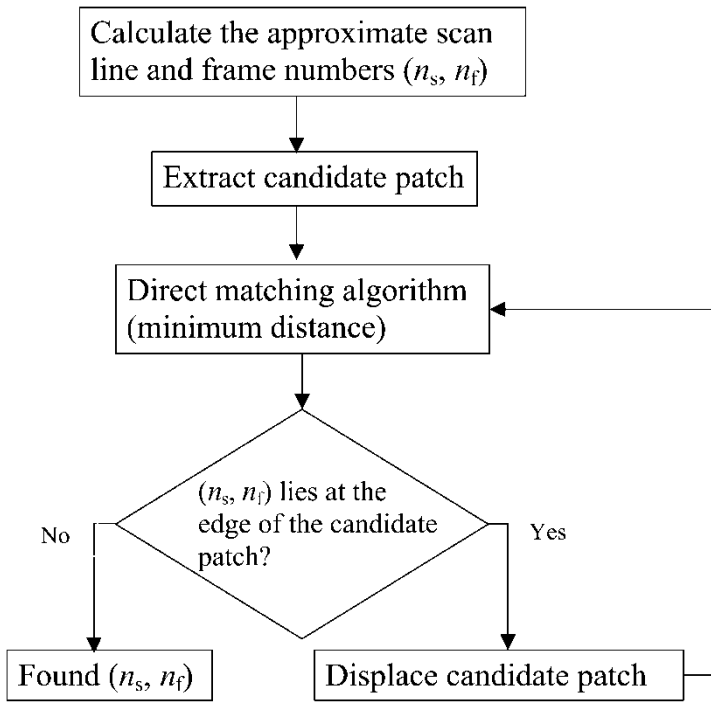
Figure 4. Flow chart for the matching of ground station in the MODIS imagery granule.

effects must be removed from the apparent reflectance. In this section, the apparent reflectance is derived from the MODIS VNIR bands. Then atmospheric effects are corrected by using the 6S radiative transfer algorithm (Tanré *et al.* 1992, Vermote *et al.* 1997a, b, c) to obtain the surface reflectance.

4.1. *Retrieval of reflectance and viewing and illumination geometrical parameters*

After the scan line number and the frame number of the pixel is found using the direct matching algorithm, the apparent spectral reflectance of band B for the pixel can be obtained with (Guenther *et al.* 1998)

$$\rho^B = R^B_{scale}\left(SI^B - R^B_{offset}\right)/\cos\theta_0 \tag{3}$$

where R^B_{scale}, R^B_{offset} are reflectance scale and reflectance offset for band B that are

Table 3. Match of the imagery pixel and position of ground station.

Day (granule)	Scan line	Frame line	Centre of pixel	Station position	Distance between (m)	Ozone (cm-atm)	Water vapour (g cm^{-2})
65	1752	789	74.1205° S, 109.665° W	74.1215° S, 109.674° W	294.869	0.2370	0.9623
70	957	643	71.7395° S, 115.135° W	71.7439° S, 115.1315° W	503.095	0.3423	1.073
78	874	1222	74.2611° S, 104.676° W	74.2554° S, 104.704° W	1053.674	0.3199	0.607

Table 4. MODIS data summary for the ground (day) station pixels.

Day (granule)	Start of the granule (UTC time)	Solar zenith	Solar azimuth	Sensor zenith	Sensor azimuth	Valid bands
65	16:15	73.758°	50.016°	10.032°	−62.632°	13
70	16:35	74.292°	50.738°	03.216°	112.082°	16
78	17:25	75.13°	25.78°	51.00°	−83.88°	20

stored as metadata attributes of SDSs. θ_0 is the solar zenith angle at the pixel. SI^B is the scaled integer value of the SDSs stored in the L1B granule files of the pixel for band B. In the case of bands 13 and 14, which are two sets of the same spectral channel—one for high gain and the other for low gain—when the two channels for each band are not saturated, the average is taken as the representative.

Viewing and illumination geometrical parameters are retrieved from the three days' granules. Results are shown in table 4. The apparent reflectances for the three stations are shown in figure 5. Table 4 also lists the valid band numbers whose SI values are usable for the station pixels. MODIS bands cover 20 VNIR bands. Bands 8–19 are for study of ocean colour, phytoplankton and biogeochemistry. These bands are generally in high gain mode, as a result the sensors of these bands are saturated for highly reflective surfaces and the SI values in L1B products are negative and unusable. For day 65's granule, usable bands include bands 1–9, bands 17–19 and band 26. For day 70's granule, only sensors of bands 13–15 are saturated because of lower ice concentration. However, for band 7 (2.13 μm) the data are unusable due to the failure of the aggregation algorithm from 500 m to 1 km spatial resolution. For day 78's granule, all of the 20 bands are usable, with no bands saturated.

4.2 Retrieval of atmospheric parameters

Atmospheric parameters, such as total ozone burden, temperature and moisture profiles and atmospheric water vapour are retrieved from MODIS MOD07_L2 products. These products are at 5 km × 5 km spatial resolution, while the reflectance value is retrieved from MODIS L1B product at 1 km spatial resolution. Just as is done for the retrieval of directional reflectance, the atmospheric parameters are retrieved (Menzel and Gumley 1998). Total ozone contents and total column precipitable water vapour retrieved from infrared channels are shown in table 3. Ozone burden ranges from 0.237 cm-atm (day 65) to 0.3423 cm-atm (day 70) and water vapour ranges from 0.607 g cm^{-2} (day 78) to 1.073 g cm^{-2} (day 70).

4.3 Atmospheric correction of retrieved reflectance from MODIS data

The retrieved apparent spectral reflectance above from MODIS data deviates from the ground reflectance due to gaseous absorption and scattering by atmospheric molecules, water vapour and aerosols. In order to obtain the ground reflectance from the apparent reflectance, atmospheric effects need to be corrected with radiative transfer models. The 6S radiative transfer model is believed to be accurate over a variety of different surfaces (Mithchell and O'Brien 1993), and thus is widely used for atmospheric correction (Stroeve *et al*. 1997, Lucht *et al*. 2000). Atmospheric correction of the MODIS satellite reflectance for this study was
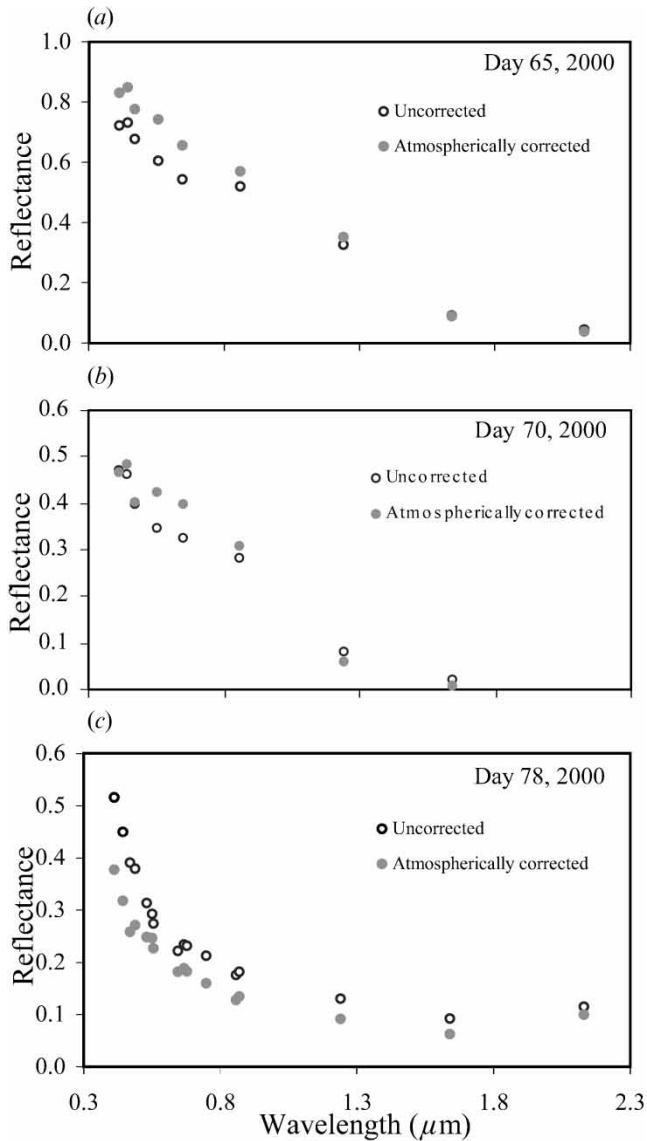
Figure 5. Comparison of bidirectional reflectances retrieved from MODIS L1B products with and without atmospheric corrections: (*a*) day 65, (*b*) day 70 and (*c*) day 78, 2000.

performed using the 6S radiative transfer model (Vermote *et al.* 1997a, b) with a few modifications. The apparent reflectance obtained in §4.1 is atmospherically corrected in the following way.

(1) The 6S algorithm is extended to include the 20 MODIS VNIR bands in our study. This involves updating and supplementing the relative spectral response (RSR) (normalized to unity at peak) for each band. Terra MODIS relative spectral response L1B LUT, which contains the in-band RSRs for each sensor of all the 36 spectral bands, can be downloaded

from the MODIS Characterization Support Team (MCST) home page (mcstftp.gsfc.nasa.gov) using the file transfer protocol (ftp) utility. For the atmospheric correction purpose, the average RSRs of all the detectors for each band is taken as the RSR for that band.

(2) The standard Arctic summer atmospheric profile (pressure, temperature, ozone and humidity) is selected as the atmospheric profile model, with the specific profile modified so that total ozone contents and total column precipitable water vapour are equal to those retrieved from the MOD07_L2 products (§4.2). Maritime aerosol model is chosen for aerosol with meteorological visibility ranging from 30 km (day 65), 15 km (day 70) to 40 km (day 78) recorded from the ship's bridge immediately before occupation of each ice station. This corresponds to the aerosol optical depth at $0.55\,\mu m$ of 0.20, 0.32 and 0.17 respectively.

(3) With the MODIS-retrieved apparent reflectance, terrestrial parameters (solar zenith and azimuth angles), viewing geometrical parameters (viewing zenith and azimuth angles) from L1B products, and atmospheric parameters (ozone burden and water content) retrieved from MOD07_L2 products as inputs, the corrected reflectance is obtained by running the 6S code band by band.

Reflectances on the three measurement sites shown in figure 1 before and after atmospheric correction are shown in figure 5. Figure 5(*a*), (*b*) and (*c*) correspond respectively to days 65, 70 and 78. For the satellite-derived reflectance on the MY ice dominant site of days 65 (figure 5(a)), the average change due to atmospheric correction is 13.8%, with the maximum change being 22.6% at band 4 ($0.555\,\mu m$) and the minimum change 2.9% at band 6 ($1.64\,\mu m$). At the site of day 70, where MY ice floated in new ice and open water background, the visibility was low compared with other days, but the correction is almost the same. The average atmospheric correction is 13.0%, with the maximum change being 25.3% at band 5 ($1.24\,\mu m$) and the minimum change 0.8% at band 8 ($0.412\,\mu m$). For day 78 with only 3.5/10 young ice concentration, the average atmospheric correction is 24.0%, with the maximum change being 33.9% at band 3 ($0.469\,\mu m$) and the minimum change 13.0% at band 7 ($2.13\,\mu m$). Reflectances of all bands shown in figure 5(*c*) after atmospheric correction are smaller than uncorrected values.

For a glacier surface, the atmospheric correction based on the Dave and Gazdag (1970) method results in a 5–20% increase in reflectance for the Landsat Thematic Mapper (TM) bands (Hall *et al*. 1990). On the sites of day 65, ground conditions were comparable to, but still more heterogeneous than, a glacier ice surface. The increase of reflectance due to atmospheric correction ranges from 2.9% to 22.6%.

5. Comparison of the *in situ* measurements with the MODIS-derived reflectance

MODIS-derived and *in situ* reflectances have been compared in order to assess the utility of the MODIS reflective bands for obtaining realistic reflectance measurements of snow and sea ice in the polar regions. From above sections, the *in situ* measured bidirectional reflectance at the three sites on sea ice floes under clear sky conditions are ice concentration weighted or corrected based on the spectral reflectance measurements of different types of ice and ice concentration observations at the measurement site. The MODIS-derived reflectances concurrently

acquired with the *in situ* measurements are atmospherically corrected, with the atmospheric parameters used for the correction retrieved from MOD07_L2 products for the same granules. Comparison of the *in situ* measurements with the satellite-derived reflectances is shown in figure 6. In this section, *in situ* reflectance is referred to the concentration corrected ground-based measurement while satellite-derived reflectance is referred to the atmospherically corrected space-based reflectance. Figure 6(*a*), (*b*) and (*c*) correspond to days 65, 70 and 78 respectively. The best agreement occurs for day 65 (figure 6(*a*)). The MODIS-retrieved reflectances are generally larger than the ground measurements for the available MODIS bands. For this site, the average difference between *in situ* and satellite-derived reflectances is 4.8% with the largest discrepancy 11.6% at band 9 (0.443 μm) and the smallest difference 0.2% at band 9 (0.858 μm). For day 70 (figure 6(*b*)), a good agreement occurs for bands in the visible regions but the agreement deteriorates at the near-infrared bands. The average difference between the ground- and space-based measurements is about 8.2%. The best agreement is within 1.2% at band 10 (0.488 μm) and the worst is as much as 25.1%, occurring at band 2 (0.858 μm). In the visible regions, the MODIS-derived reflectances are larger than the *in situ* measurements, but the differences are small. In the near-infrared regions, the MODIS-derived reflectances are smaller than the ground measurements, and the differences are much larger than those in the visible bands. In the case of day 78 (figure 6(*c*)), the MODIS-retrieved reflectances in the visible spectrum regions are larger while in the near-infrared regions smaller than the *in situ* measured reflectances. For this site, the average difference between the *in situ* and satellite-derived reflectances is 6.2%, with the largest discrepancy (16.9%) at band 8 (0.412 μm) and the smallest discrepancy (0.8%) at band 4 (0.555 μm).

One of the possible error sources is the error in estimation of concentrations of different ice types. To see the effect of the errors in ice concentration estimate on the comparison of the MODIS-derived and *in situ* reflectances, the site of day 78 is taken as an example. As there was only one type of ice available at the site, a sensitivity study of the reflectance to the ice concentration should be more straightforward than other cases. Had the ice concentration been 5/10 instead of 3.5/10, the average difference between the *in situ* and space measurements would be increased from 6.2% to 22.4%, and the largest discrepancy (30.1%) occurs at band 2 (0.858 μm) and the smallest discrepancy (12.5%) at band 8 (0.412 μm). This result is shown in figure 7. Much worse agreement occurs when the ice concentration is 5/10. Because of the very complicated topography and ice types mixture, errors in ice classification may contribute significantly to the discrepancy.

6. Discussion and conclusions

Within the present investigation, bidirectional reflectance and spectral albedo measurements were performed on the snow and sea ice surface in the Amundsen Sea, Antarctica, coincident with the MODIS overpasses, to assess the discrepancy between the *in situ* and the MODIS-derived surface reflectance of the snow and sea ice and thus allow for assessment of the accuracy of a satellite-retrieved albedo. The *in situ* reflectance measurements were ice concentration corrected so that the reflectance of the 1 km simulated ground pixel was compared with the atmospheric corrected reflectance retrieved from the MODIS 1 km products. An atmospheric
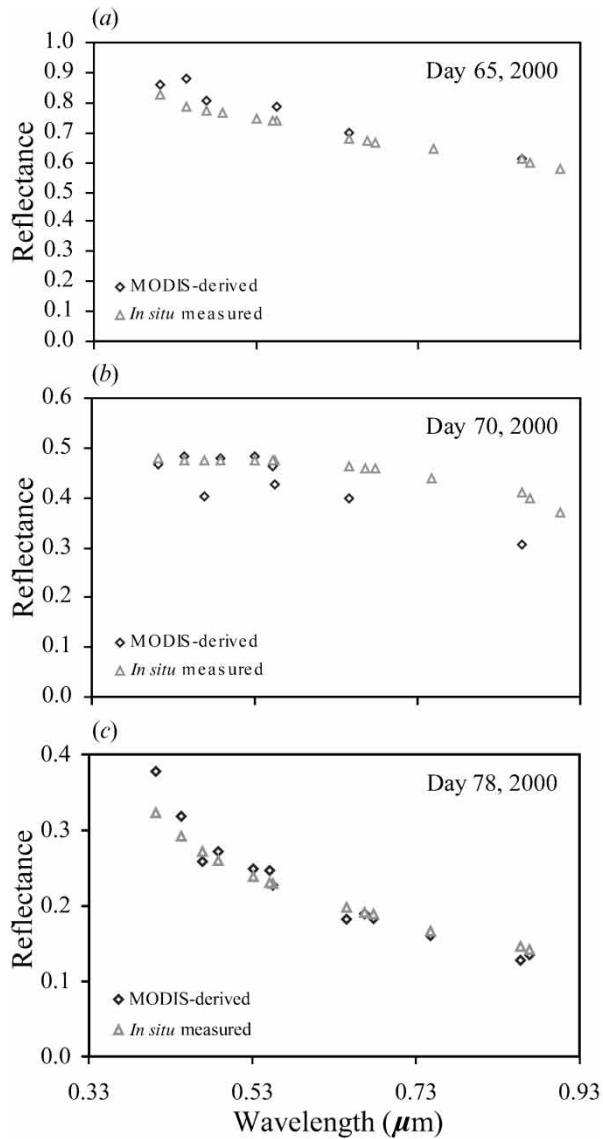
Figure 6.   Comparison of bidirectional reflectance of *in situ* measurements and MODIS-
derived data: (*a*) day 65, (*b*) day 70 and (*c*) day 78, 2000.

correction of the MODIS data was performed using the 6S radiative transfer model
with the extension to all MODIS solar spectral bands.

A sensitivity study of satellite-retrieved reflectances for clear sky conditions was
conducted by Stroeve *et al.* (1997) using the 6S model. A 50% change in aerosol
amount can lead to errors of as much as 3.3%, while for 50% uncertainty in ozone
concentration the error is about 1.5%. Uncertainties in water vapour content have
the least effect on the satellite measurement. Discrepancy between satellite-derived
and *in situ* measurements is common. For instance, the Advanced Very High
Resolution Radiometer (AVHRR) polar pathfinder-derived surface albedos and the
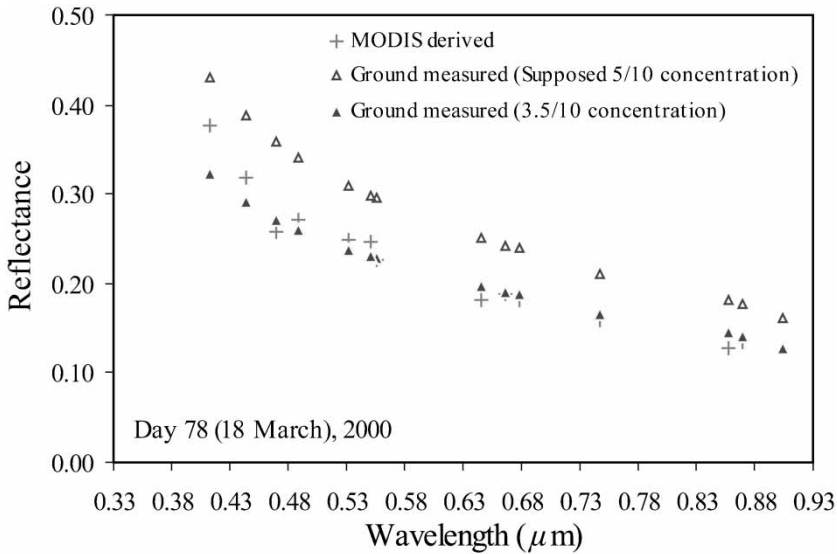
Figure 7. Dependence of *in situ* bidirectional reflectance on ice concentrations when there is only one ice type as on the site of day 78, 2000. Atmospherically corrected bidirectional reflectance derived from MODIS data of day 78 is also shown for comparison.

ground-measured values differ on average by 10%, with worst cases exceeding 38% (Stroeve *et al*. 2001).

The cruise we participated in was a multi-purpose mission; the time allocated to each science group was limited at each ice station. We had not been able to make surface reflectance measurements on all the main ice types at each ice station. To estimate the possible effect of the variation of the spectral albedo of young white ice on the ice concentration corrected *in situ* reflectance for the ice station of day 65, we take the maximum deviation of spectral albedo of MY ice (see §2.1) as the maximum representative range of variation for young white ice. We take MODIS band 4 (553.6 nm) as an example; the error resulting from the variation of spectral reflectance of young white ice is expected to be within $\pm 1.0\%$. Reflectance of new ice (5–10 cm) is generally very low (0.2–0.3). When the measurements for the MODIS validation were made on the dominant and most reflective MY ice, errors resulting from the uncertainty of spectral albedo of new ice (5–10 cm) are even less. For instance, the same analysis for young white ice was applied to the new ice for the ice station of day 70 and the error is within $\pm 0.83\%$ of the concentration corrected reflectance of band 4. Analyses for the other bands resulted in similar conclusions. From these analyses, we can see that the errors resulting from the variation of spectral albedo of the second or tertiary ice type are within $\pm 1.0\%$.

Anisotropic reflectance is believed to be an important source in errors in the satellite-retrieved albedo data (Steffen 1996, Stroeve *et al*. 1997, Knap and Reijmer 1998, Jin and Simpson 2000), thus it is routinely corrected for the retrieval of the surface albedo from satellite measurements. However, for this study, the comparison is on the bidirectional reflectance, and the illumination and viewing geometry were the same for both the satellite and *in situ* measurements. Anisotropy

was already included in both the MODIS-retrieved and *in situ* data. Errors due to anisotropy occur when the surface reflectance is ice concentration corrected using spectral albedo (isotropic reflectance) instead of bidirectional reflectance for the secondary and tertiary ice types as was done in §2.2. However, anisotropic correction is still controversial (De Abreu *et al*. 1994). In fact, application of the anisotropic correction factor (Taylor and Stowe 1984) obtained at TOA to ground reflectance can result in corrected albedo exceeding 1, especially for very reflective surfaces such as snow-covered FY, MY and land-fast ice. Given the heterogeneous features of the ice surface in the Amundsen Sea, Taylor and Stowe's (1984) method may not be appropriate (De Abreu *et al*. 1994). As noted in §2.2, errors due to anisotropy depend largely on the representativity of the primary ice type within the simulated pixel. The more representative the primary ice type on which the reflectance is measured, the fewer errors due to the uncertainty in anisotropy as were the case of days 65 and 78, 2000.

The main challenge in satellite date validation is to attain adequate ground sampling of observed bio- and/or geophysical variables that exhibit spatial and temporal variance at the sub-pixel scale of a satellite sensor. This problem is even more serious for the sea ice pack in the polar oceans than for land surface because of the constant dynamical behaviours of sea ice in the ice pack (Hibler 1979, Geiger *et al*. 1998). For validation of sea ice products, one important source of errors may be from the uncertainty of ice concentration of different ice types. For instance, taking the atmospheric parameter of day 78 and supposing the surface consists of only young grey ice and open water, an assumed 5/10 of ice concentration instead of 3.5/10 can result in an error of as much as 33.5%. Besides, the ice concentration correction was made with the albedo of the minor ice types taken from the other stations. This can result in errors that depend on the surface composition. The ice concentration was estimated from the research vessel-based observations and field digital images. An alternative method of classification of the ground surface types is expected if higher spatial resolution multispectral images such as TM and/or Enhanced Thematic Mapper (ETM)+ or Advanced Spaceborne Thermal Emission and Reflection Radiometer (ASTER) data are available so that by appropriate classification algorithms the coarse spatial resolution pixel can be spectrally unmixed (Barnsley *et al*. 2000, Lucht *et al*. 2000). Considering the validation is on the sea ice, which can drift at a velocity from 4.3 km/day to 21.6 km/day due to winds and currents (Kottmeier *et al*. 1992), we need near-perfect concurrent acquisitions of the high-resolution images for MODIS validation. The probability that an ice station covered by MODIS could also be semi-concurrently covered by a sensor with a narrower swath equals the ratio of the swath of that particular sensor over that of MODIS. It is generally small. For instance, the probability was around 8% (185 km/2330 km) for Landsat sensors. As for high resolution sensor onboard the same space platform, for instance, ASTER onboard Terra, the probability was around 2.6% (60 km/2330 km) (the side-looking capability of ASTER is not considered due to the unpredictability of the ship's position on a given date). For a specific ice station, the location of the station on a MODIS image is indicative of the possible availability of an ASTER image. On day 70, the frame number (643, see table 3) is close to the central frame (677). This means there might be a concurrent ASTER image to cover the station if ASTER was on at the time. For days 65 and 78, the availability of ASTER images is zero because the ice stations

were far from the central frame of the MODIS image. Search of the Landsat and ASTER archives (http://edcsns17.cr.usgs.gov/EarthExplorer, and http://asterweb. jpl.nasa.gov/gettingdata) indicated that no high-resolution satellite data such as TM or ETM+ from Landsat-5 and Landsat-7 and ASTER data were concurrently or semi-concurrently (within three days) acquired with the MODIS data used for the present study. This illustrates another difficulty in validating sea ice products, i.e. the less availability of concurrent high-resolution satellite data usable for unmixing low-resolution satellite data.

A good agreement between the *in situ* and MODIS-derived reflectances depends on the representativeness of the ice station in the corresponding MODIS pixel, appropriate correction of atmosphere, ground anisotropy, inhomogeneity, variability of topography, and the accuracy of the sub-pixel proportions of the ice types in the pixel. Comparison between the MODIS-derived and *in situ* reflectances shows that a good agreement was found when the ice concentration was 10/10 with the most coverage similar in reflectivity (as on day 65, with discrepancy range being 0.2–11.6%, and the average agreement within 4.8%) or when the pixel was one ice-type dominated and the measurement was taken on the dominant ice floe (as on day 78) (with discrepancy being 0.8–16.9%, average difference within 6.2%). For the pixel that contained more than one ice-type (day 70) that is substantially distinct in surface reflectance, worse agreement (discrepancy range 0.8–25.3%, average discrepancy as much as 13.0%) occurred. With the ground site very inhomogeneous and surface topography very variable, the discrepancy can be as large as 30% (Hall *et al.* 1990). Comparison for such conditions can be very difficult. We therefore concluded that:

(1) The best agreement between the *in situ* and MODIS measurements was found when the ground had 10/10 ice concentration or was one-ice-type dominant. A good comparison between the *in situ* and satellite-retrieved reflectances is expected on a large and homogeneous ice floe under clear sky conditions.

(2) Simultaneousness is a necessity for the *in situ* and space-based measurements to avoid ground data drift when validation is on a moving surface feature such as sea ice. There are no 'permanent' ground data in validation of sea ice products. Synchronization is more imperative for the sea ice product validation than for other land surface products where 'permanent' ground data exist.

(3) To avoid errors resulting from ice concentration correction, an accurate determination of ice concentration is important in deriving ground reflectance of a simulated pixel from the *in situ* measurements when a pixel covers several optically distinctive ice types. It is expected that the more homogeneous the ground surface and the less variable the ground topography, the more comparability there is between the *in situ* and satellite-derived reflectance.

References

ALLISON, I., BRANDT, R. E., and WARREN, S. G., 1993, East Antarctic sea ice: albedo, thickness distribution, and snow cover. *Journal of Geophysical Research*, **98**, 12 417–12 429.

BARNSLEY, M. J., HOBSON, P. D., HYMAN, A. H., LUCHT, W., MULLER, J.-P., and STRAHLER, A. H., 2000, Characterizing the spatial variability of broadband albedo in a semidesert environment for MODIS validation. *Remote Sensing of Environment*, **74**, 58–68.

DAVE, J. V., and GAZDAG, J., 1970, A modified Fourier transform method for multiple scattering calculations in a plane-parallel atmosphere. *Applied Optics*, **9**, 1457–1466.

DE ABREU, R. A., KEY, J., MASLANIK, J. A., SERREZE, M. C., and LEDREW, E. F., 1994, Comparison of *in situ* and AVHRR-derived broadband albedo over Arctic sea ice. *Arctic*, **47**, 288–297.

DOZIER, J., and MARKS, D., 1987, Snow mapping and classification from Landsat Thematic Mapper data. *Annals of Glaciology*, **9**, 97–103.

DUGUAY, C. R., and LEDREW, E. F., 1992, Estimating surface reflectance and albedo from Landsat-5 Thematic Mapper over rugged terrain. *Photogrammetric Engineering and Remote Sensing*, **58**, 551–558.

ELSON, L., ALLEN, M., GOLDSMITH, J., ORTON, M., and WEIBEL, W., 2000, An example of a network-based approach to data access, visualization, interactive analysis and distribution. *Bulletin of the American Meteorological Society*, **81**, 555–566. Documentation and software of WebWinds are available online at http://webwinds.jpl.nasa.gov.

GEIGER, C. A., HIBLER, W. D. III, and ACKLEY, S. F., 1998, Large scale sea ice drift and deformation: comparison between models and observations in the western Weddell Sea during 1992. *Journal of Geophysical Research*, **103**, 21 893–21 913.

GOGINENI, S. P., MOORE, R. K., GRENFELL, T. C., BARBER, D. G., DIGBY, S., and DRINKWATER, M., 1992, The effects of freeze-up and melt processes on microwave signatures. In *Microwave Remote Sensing of Sea Ice* (edited by F. D. Carsey, Geophysical Monograph 68, Washington, DC: American Geophysical Union), pp. 329–341.

GRATTON, D. I., HOWART, P. J., and MARCEAU, D. J., 1993, Using Landsat-5 Thematic Mapper and digital elevation data to determine the net radiation field of a mountain glacier. *Remote Sensing of Environment*, **43**, 315–331.

GREUELL, W., and DE RUYTER DE WILDT, M., 1999, Anisotropic reflectance by melting glacier ice: measurements and parameterizations in Landsat TM bands 2 and 4. *Remote Sensing of Environment*, **70**, 265–277.

GUENTHER, B., GODDEN, G. D., XIONG, X., KNIGHT, E. J., QIU, S.-Y., MONTGOMERY, H., HOPKINS, M. M., KHAYAT, M. G., and HAO, Z., 1998, Prelaunch algorithm and data format for the Level 1 calibration products for the EOS-AM1 Moderate Resolution Imaging Spectroradiometer (MODIS). *IEEE Transactions on Geoscience and Remote Sensing*, **36**, 1142–1151.

HALL, D. K., BINDSCHADLER, R. A., FOSTER, J. L., CHANG, A. T. C., and SIDDALINGAIAH, H., 1990, Comparison of *in situ* and satellite-derived reflectance of Forbindels glacier, Greenland. *International Journal of Remote Sensing*, **11**, 493–504.

HALL, D. K., FOSTER, J. L., and CHANG, A. T. C., 1992, Reflectance of snow as measured

in situ and from space in sub-arctic areas in Canada and Alaska. *IEEE Transactions on Geoscience and Remote Sensing*, **30**, 634–637.

HIBLER, W. D. III, 1979, Ice dynamics. Cold Regions Research and Engineering Laboratory (CRREL) Monograph 84-3, Hanover, New Hampshire, USA.

JIN, Z., and SIMPSON, J., 2000, Bidirectional anisotropic reflectance of snow and sea ice in AVHRR channel 1 and channel 2 spectral regions—Part II: Correction applied to imagery of snow on sea ice. *IEEE Transactions on Geoscience and Remote Sensing*, **38**, 999–1015.

KNAP, W. H., and OERLEMANS, J., 1996, The surface albedo of the Greenland ice sheet: satellite derived and *in situ* measurements in the Sondre Stromfjord area during the 1991 melt season. *Journal of Glaciology*, **42**, 364–374.

KNAP, W. H., and REIJMER, C. H., 1998, Anisotropy of the reflected radiation field over melting glacier ice: measurements in Landsat TM bands 2 and 4. *Remote Sensing of Environment*, **65**, 93–104.

KNAP, W. H., REIJMER, C. H., and OERLEMANS, J., 1999, Narrowband to broadband conversion of Landsat-TM glacier albedos. *International Journal of Remote Sensing*, **20**, 2091–2110.

KOEPKE, P., 1989, Removal of atmospheric effects from AVHRR albedos. *Journal of Applied Meteorology*, **28**, 1341–1348.

KOTTMEIER, C., OLF, J., FRIEDEN, W., and ROTH, R., 1992, Wind forcing and ice motion in the Weddell sea region. *Journal of Geophysical Research*, **97**, 20 373–20 383.

LILJEQUIST, G. H., 1956, Energy exchange of an Antarctic snowfield, short-wave radiation (Maudheim, $71°03'$ S, $10°56'$ W). *Norwegian–British–Swedish Antarctic Expedition, 1949–52, Scientific Results*, vol. II, part 1A (Oslo: Norsk Polarinstitutt).

LUCHT, W., HYMAN, A. H., STRAHLER, A. H., BARNSLEY, M. J., HOBSON, P., and MULLER, J.-P., 2000, A comparison of satellite-derived spectral albedos to ground-based broadband albedo measurements modeled to satellite spatial scale for a semidesert landscape. *Remote Sensing of Environment*, **74**, 85–98.

MENZEL, W. P., and GUMLEY, L. E., 1998, MODIS atmospheric profiles retrieval algorithm theoretical basis document. ATBD-MOD-07, NASA Goddard Space Flight Center, pp. 1–38. Available online at http://ltpwww.gsfc.nasa.gov/MODIS-Atmosphere/ _docs/atbd_mod07.pdf.

MITHCHELL, R. M., and O'BRIEN, D. M., 1993, Correction of AVHRR shortwave channels for the effects of atmospheric scattering and absorption. *Remote Sensing of Environment*, **46**, 129–145.

NISHIHAMA, M., WOLFE, R., SOLOMON, D., PATT, F., BLANCHETTE, J., FLEIG, A., and MASUOKA, E., 1997, MODIS Level 1A Earth location: algorithm theoretical basis document version 3.0, SDST-092, August 1997. Available online at http://eospso. gsfc.nasa.gov/ftp_ATBD/REVIE W/MODIS/ATBD-MOD-28/atbd-mod-28.pdf.

PATT, F. S., WOODWARD, R. H., and GREGG, W. W., 1997, An automated method for navigation assessment for Earth survey sensors using island targets. *International Journal of Remote Sensing*, **18**, 3311–3336.

REIJMER, C. H., BINTANJA, R., and GREUELL, W., 2001, Surface albedo measurements over snow and blue ice in thematic mapper bands 2 and 4 in Dronning Maud Land, Antarctica. *Journal of Geophysical Research*, **106**, 9661–9672.

SCHLATTER, T. W., 1972, The local surface energy balance and subsurface temperature regime in Antarctica. *Journal of Applied Meteorology*, **11**, 1048–1062.

SELLERS, W. D., 1969, A global climate model based on the energy balance of the Earth–Atmosphere system. *Journal of Applied Meteorology*, **8**, 392–400.

STEFFEN, K., 1997, Effect of solar zenith angle on snow anisotropic reflectance. *IRS'96: Current Problems in Atmospheric Radiation. Proceedings of the International Radiation Symposium, Fairbanks, Alaska, 19–24 August 1996*, edited by W. L. Smith and K. Stamnes (A. Deepak Publishing), pp. 41–44.

STROEVE, J., NOLIN, A., and STEFFEN, K., 1997, Comparison of AVHRR-derived and *in situ* surface albedo over the Greenland ice sheet. *Remote Sensing of Environment*, **62**, 262–276.

STROEVE, J. C., BOX, J. E., FOWLER, C., HARAN, T., and KEY, J., 2001, Intercomparison

between *in situ* and AVHRR polar pathfinder-derived surface albedo over Greenland. *Remote Sensing of Environment*, **75**, 360–374.

TANRÉ, D., HOLBEN, B. N., and KAUFMAN, Y. J., 1992, Atmospheric correction algorithm for NOAA-AVHRR products: theory and application. *IEEE Transactions on Geoscience and Remote Sensing*, **30**, 231–250.

TAYLOR, V. R., and STOWE, L. L., 1984, Reflectance characteristics of uniform Earth and cloud surfaces derived from Nimbus 7 ERBE. *Journal of Geophysical Research*, **89**, 4987–4996.

VERMOTE, E. F., SALEOUS, N. E., JUSTICE, C. O., KAUFMAN, Y. J., PRIVETTE, J. L., REMER, L., ROGER, J. C., and TANRÉ, D., 1997a, Atmospheric correction of visible to middle-infrared EOS-MODIS data over land surface: background, operational algorithm and validation. *Journal of Geophysical Research*, **102**, 17 131–17 141.

VERMOTE, E., TANRÉ, D., DEUZÉ, J. L., HERMAN, M., and MORCRETTE, J. J., 1997b, Second simulation of the satellite signal in the solar spectrum: an overview. *IEEE Transactions on Geoscience and Remote Sensing*, **35**, 675–686.

VERMOTE, E., TANRÉ, D., DEUZÉ, J. L., HERMAN, M., and MORCRETTE, J. J., 1997c, Second simulation of the satellite signal in the solar spectrum (6S), 6S user guide version 2, July 1997. Code and documentaions are available online at ftp://kratmos.gsfc.gov/pub/6S.

WARREN, S. G., BRANDT, R. E., and HINTON, P. O., 1998, Effect of surface roughness on bidirectional reflectance of Antarctic snow. *Journal of Geophysical Research*, **103**, 25 789–25 807.

WORBY, A., and ALLISON, I., 1999, A technique for making ship-based observations of Antarctic sea ice thickness and characteristics, part I, Observational techniques and results. In *Research Report*, vol. 14 (Hobart, Tasmania: Antarctic CRC), pp. 1–23.

ZHOU, X., and LI, S., 2000, Measurement of BRDF of snow and sea ice in the Ross and Amundsen Seas by the visible and near-infrared channels of MODIS. *Proceedings of IGARSS'00 Symposium, Taking the Pulse of the Planet: The Role of Remote Sensing in Managing the Environment, Hawaii, USA, 24–28 July 2000* (Piscataway, NJ: IEEE), pp. 1567–1569.

ZHOU, X., LI, S., and MORRIS, K., 2001, Measurement of all-wave and spectral albedos of snow-covered summer sea ice in the Ross Sea, Antarctica. *Annals of Glaciology*, **33**, 267–274.